Theoretical analysis and experiment of subwavelength structure-integrated red AlGaInP light-emitting diodes for uniform field distribution and enhanced light extraction efficiency

Gil Ju Lee and Young Min Song[a]
Department of electronics engineering, Pusan National University, 2 Busandaehak-ro 63 beon-gil, Geumjeong-gu, Busan, 609-735, Republic of Korea

(Received 18 November 2015; accepted 25 February 2016; published online 3 March 2016)

We report theoretical and experimental analysis of antireflective subwavelength structures (SWSs) on GaP substrates to enhance the light output with a uniform light distribution of AlGaInP-based red light-emitting diodes (LEDs). Scaling issues on the optical performance are analyzed by the calculation results from finite-difference time-domain (FDTD) and rigorous coupled-wave analysis (RCWA) methods. The optical simulation reveals that SWSs with a period of 100–150 nm achieve highest optical output power, while maintaining a uniform light field distribution, in the subwavelength regime. To validate our theoretical results, disordered SWSs with a tapered shape were fabricated on a GaP layer of AlGaInP red LEDs by lithography-free dry etching of Ag nanoparticles. The SWS-integrated LED shows a uniform light output distribution with an improved light output power compared with the conventional LED. © *2016 Author(s). All article content, except where otherwise noted, is licensed under a Creative Commons Attribution (CC BY) license (http://creativecommons.org/licenses/by/4.0/).* [http://dx.doi.org/10.1063/1.4943529]

I. INTRODUCTION

Today, light-emitting diodes (LEDs) offer a significant promise for efficient energy usage in lighting and display applications. Although the external quantum efficiency (EQE) of solid state LEDs has significantly improved over the last few decades, it remains one of the most important figures of merit of LEDs. To date, various approaches have been explored to improve the EQE, such as surface roughening or texturing, two-dimensional or three-dimensional nanophotonic structures, and reflecting mirrors.[1–5] Along with advanced fabrication techniques, subwavelength structures (SWSs) with a tapered profile were also explored for extracting more light into the surrounding.[6–9] These inclined structures, called 'moth eye' structures, can reduce the unwanted surface Fresnel reflection over a broad wavelength and wide angular ranges when the period of the structure is much smaller than the optical wavelength. Recently, SWS-integrated LEDs showed a significant improvement in light extraction because of the introduction of a graded-index media in the semiconductor/air interface.[10–13] The combination of microstructures and SWSs were also reported to maximize the light extraction efficiency by reducing both the total internal reflection (TIR) loss and Fresnel reflection loss.[2,14,15] Although various structures based on SWSs and graded-index media have been developed for high efficiency LEDs, there have been relatively fewer studies on the comprehensive optical modeling of SWS-integrated LEDs.

In this study, we have systematically investigated the light extraction characteristics of SWS-integrated AlGaInP-based red LEDs with different periods/heights based on three-dimensional finite-difference time-domain (FDTD) and rigorous coupled-wave analysis (RCWA) methods. Various calculation results on electrical field distributions, far-field patterns, angle-dependent transmittances, and

[a]Electronic mail: ysong@pusan.ac.kr

 ©Author(s) 2016.

diffraction energy distributions support our analysis. Optimum periods were determined from the estimation of light output power for SWS-integrated LEDs with different geometries through the calculation of efficiency of out-coupled light in steady state. To validate the results of our analysis, we demonstrate a fabricated SWS-integrated red AlGaInP LED with a nanoscale pattern. We further discuss fabrication details and measurement results of the fabricated LEDs.

II. STRUCTURES AND SIMULATION METHOLOGY

Both the uniformity of the radiation pattern and high EQE are important in some applications such as displays. In order to use SWS-integrated LEDs for such applications, there should be only zeroth-order diffraction, which strongly depends upon the period of the structures.[16] We first simulated the light output power and electric field distribution of the SWS-integrated LEDs based on the FDTD method. Figure 1(a) shows a schematic illustration of the computation domain consisting of GaP parabolic structures with a hexagonal lattice on the LED stacks (n-GaP (1 μm)/multiple quantum well (MQW) (0.1 μm)/p-GaAs (0.16 μm)). The refractive indices of all materials in our study were taken from the library of the simulation software (RSoft Design Group, USA). The lateral dimension of the computation domain is 9 μm × 9 μm, surrounded by a perfectly matched layer (PML) generating reliable calculation results. Although a distributed Bragg reflector (DBR) is commonly located at the bottom side of LEDs, we have only used the PML in our simulations for simplicity. This has made it difficult to consider the edge emission of LEDs. The influence of edge emissions can be considered in the ray tracing–based calculations.[17] A transverse magnetic (TM)-polarized point source was located in the active layer plane (i.e., MQW layer) across the domain, and it was driven by a continuous sinusoidal wave at a wavelength of 633 nm. For comparison, we selected two distinct periods, namely, 150 nm and 600 nm, by considering the refractive index of the GaP and incident wavelength. As a reference, we also conducted the calculation for conventional LEDs with flat surfaces.

Figure 1(b) shows the monitored light output power for three different LEDs (i.e., conventional (black line) and SWSs with a period of 150 nm (red line) and 600 nm (blue line)). The simulation

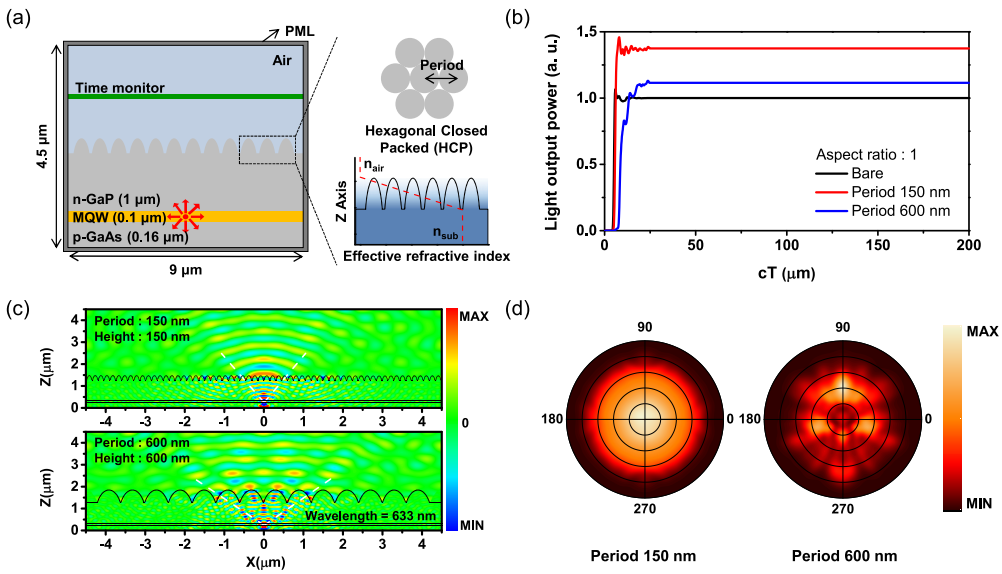

FIG. 1. (a) Schematic of the 3D FDTD computational domain for LEDs with close-packed parabolic nanostructures. In the SWSs region, parabolic SWSs have a linearly graded refractive index profile. (b) Calculated light output power of the SWSs on GaP substrate with different periods for dipole source by time monitor. Aspect ratio of the nanostructures was set to 1.0. As a reference, calculation results for GaP substrate with flat surface (i.e. bare substrate) are also included. (c) Calculated electric field distribution of the SWSs on GaP substrate at a wavelength of 633 nm for a period of 150 nm and 600 nm, respectively, in the TM mode. (d) Simulated 3D far-field patterns for a period of (left) 150 nm and (right) 600 nm at a wavelength of 633 nm.

result clearly shows that the light output power of SWS-integrated LEDs is greater than that of the bare structure. For the SWSs with a period of 150 nm, the light output enhancement is attributed to the graded refractive index of the parabolic SWSs. The electric field profiles, shown in Fig. 1(c), also support this behavior. The light radiation angle of SWS LEDs with a period of 150 nm is the same as that of bare LEDs. On the contrary, the SWSs with a period of 600 nm exhibit distinct diffraction patterns with a widened radiation angle. These results show that the textured substrate of LEDs seems to improve the EQE regardless of the size of structure; however, there is a drastic difference between the SWSs with a period of 150 nm and 600 nm in terms of the light distribution. We calculated far-field patterns (Fig. 1(d)) emitted by the LEDs, which are more relevant to the optical characteristics of actual devices. In this calculation, we used an incoherent and pulse point source with a Gaussian spectrum, considering the light emission spectra of the LEDs. The calculated far-field patterns clearly show the uniformity difference between the LEDs with a period of 150 nm and 600 nm. These results show that the structure with a large period is not suitable for applications that require uniform light emissions.

To observe the transmittance enhancement of the SWSs and distribution of the transmission efficiencies for each diffraction order, we conducted simulations based on the three-dimensional RCWA method. In overall calculations, ninth diffraction orders were used to calculate the diffraction efficiency for an accurate simulation. Figure 2 shows (a) the calculated transmittance and (b) the distribution of the transmitted diffraction efficiencies of the SWSs with a period of 150 nm and 600 nm, respectively. Fig. 2(a)-(i) shows that the SWSs with the period of 150 nm yield a transmittance of ~99% because of the graded refractive index profiles, while the transmittance is only ~74% for the bare structure at normal incidence at a wavelength of 633 nm (inset of Fig. 2(a)-(i)). Because of the homogeneity of SWSs with the period of 150 nm, the zero-order diffraction exists but is totally reflected above the critical angle, as indicated in (i) and (ii) of Fig. 2(b). As the incident angle increases, the difference in transmittance between transverse electric (TE) and TM tends to increase. The maximum difference for the SWSs with the period of 150 nm is ~7.4% at the incidence angle of 17°, whereas that for the bare surface is ~73.8% at the same incidence angle. These results show the polarization-independent antireflection performance of parabolic SWSs. For the SWSs with the period of 600 nm (Fig. 2(a)-(ii)), a greater part of the transmitted light is attributed to

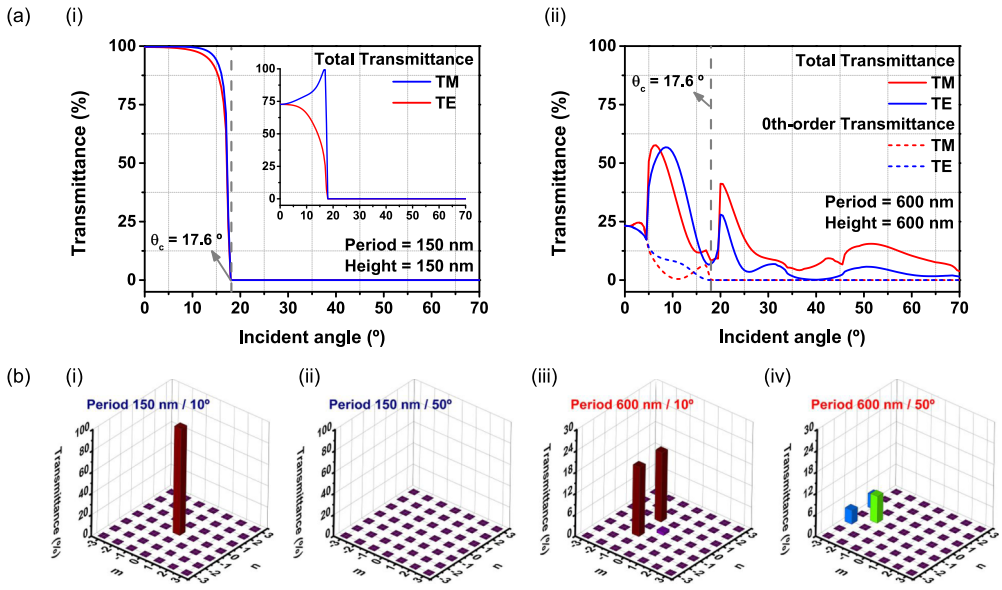

FIG. 2. (a) Calculated transmittance of the GaP with SWSs as a function of incident angle at a wavelength of 633 nm: (i) a period of 150 nm and (ii) a period of 600 nm. Inset: calculated transmittance of the bare LEDs. (b) Distribution of the transmitted diffraction efficiencies of SWSs with a period of 150 nm and 600 nm for TM polarized light: (i) a period of 150 nm and an incidence angle of 10°, (ii) a period of 150 nm and an incidence angle of 50°, (iii) a period of 600 nm and an incidence angle of 10°, (iv) a period of 600 nm and an incidence angle of 50°.

higher order diffraction occurring above the critical angle. The diffraction order tends to increase as the incident angle increases for the SWSs with a period of 600 nm ((iii) and (iv) of Fig. 2(b)).

As indicated in Fig. 2(b), (−1, −1) and (−1, 1) orders first appear as the higher diffraction orders. The higher order diffraction over second order is generated as the incident angle increases. The critical dimensions of the SWSs for satisfying the zeroth-order condition can be found by solving the 2D grating equation. The 2D grating equation is given by Ref. 18

$$n_t \sin\theta_{mn} \cos\phi_{mn} = n_i \sin\theta_i \cos\phi_i + \frac{m\lambda}{\Lambda_x} \tag{1}$$

$$n_t \sin\theta_{mn} \sin\phi_{mn} = n_i \sin\theta_i \sin\phi_i + \frac{n\lambda}{\Lambda_y} \tag{2}$$

where n_t and n_i are the refractive indices of the transmitted medium and incident medium, respectively. θ_i is the polar incidence angle, and ϕ_i is the azimuthal incidence angle. Λ_x and Λ_y are the grating periods along the x and y directions, respectively, and λ is the wavelength of the incident light. By solving the 2D grating equation for the six-fold close-packed array ($\Lambda_y = \sqrt{3}\Lambda_x$) on the GaP substrate using MATLAB, we obtained the minimum normalized wavelength (λ/Λ_x) with the diffraction polar angle of (−1,−1) order, which is perpendicular to the z axis (Fig. 3(a)). In this calculation, we only considered (−1,−1) diffraction order because of the symmetry between (−1,−1) and (−1,1) orders on the azimuthal angle. White region in Fig. 3(a) indicates that the transmitted light by (−1,−1) order is not allowed to propagate into the air regardless of the normalized wavelength. If the normalized wavelength is larger than the minimum value at each incident angle in Fig. 3(a), there is no higher order diffraction. For example, if λ/Λ_x is larger than the value of point A (i.e., 3.06) in Fig. 3(a), the zeroth-order regime is ensured from the normal to ~50°, and the first graph of Fig. 3(b) shows this result. The minimum normalized wavelength for satisfying zeroth-order regime increases as the polar incidence angle is increased. Because the period is the denominator of the normalized wavelength, the period should be decreased for maintaining the zeroth-order regime as the polar incidence angle is increased. Fig. 3(b) shows the transmittance curves of the SWSs on GaP substrate for four points in Fig. 3(a). The period of 207 nm corresponds to the value of point A, 3.06, at the wavelength of 633 nm. The transmittance of period 207 nm shows that there is a higher order diffraction above θ_i =~ 50°. Other periods that correspond to B, C, and D in Fig. 3(a) also show similar tendency (Fig. 3(b)). The maximum transmittances of (−1,−1) order of the SWSs with a period of 207 nm, 190 nm, 180 nm, and 173 nm on the GaP substrate were 33.09%, 22.06%, 20.15%, and 15.15%, respectively, at the wavelength of 633 nm. For the period of 173 nm, transmittances except for the peak point are nearly zero. Thus, the SWSs with the period of 173 nm on GaP substrate can be considered as the practical zeroth-order regime. This indicates that

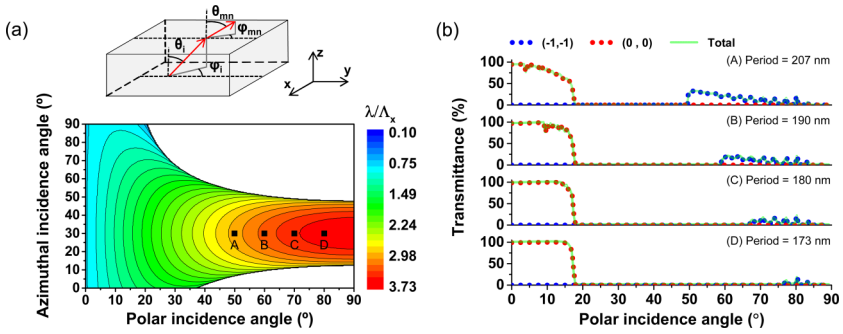

FIG. 3. (a) The contour plot of minimum normalized wavelength (λ/Λ_x) with $\theta_{-1,-1} = -90°$ as functions of azimuthal and polar incidence angles. The white region indicates that the light transmitted by (−1,−1) order is not allowed to propagate into the air regardless of the normalized wavelength. The point values of normalized wavelength in the contour plot are 3.06, 3.34, 3.53, and 3.67 for A, B, C, and D, respectively. (b) Transmittance curves of the SWSs on a GaP substrate with a period of 207 nm (A), 190 nm (B), 180 nm (C), and 173 nm (D) as a function of the polar incidence angle at the wavelength of 633 nm for the azimuthal incidence angle of 30°.

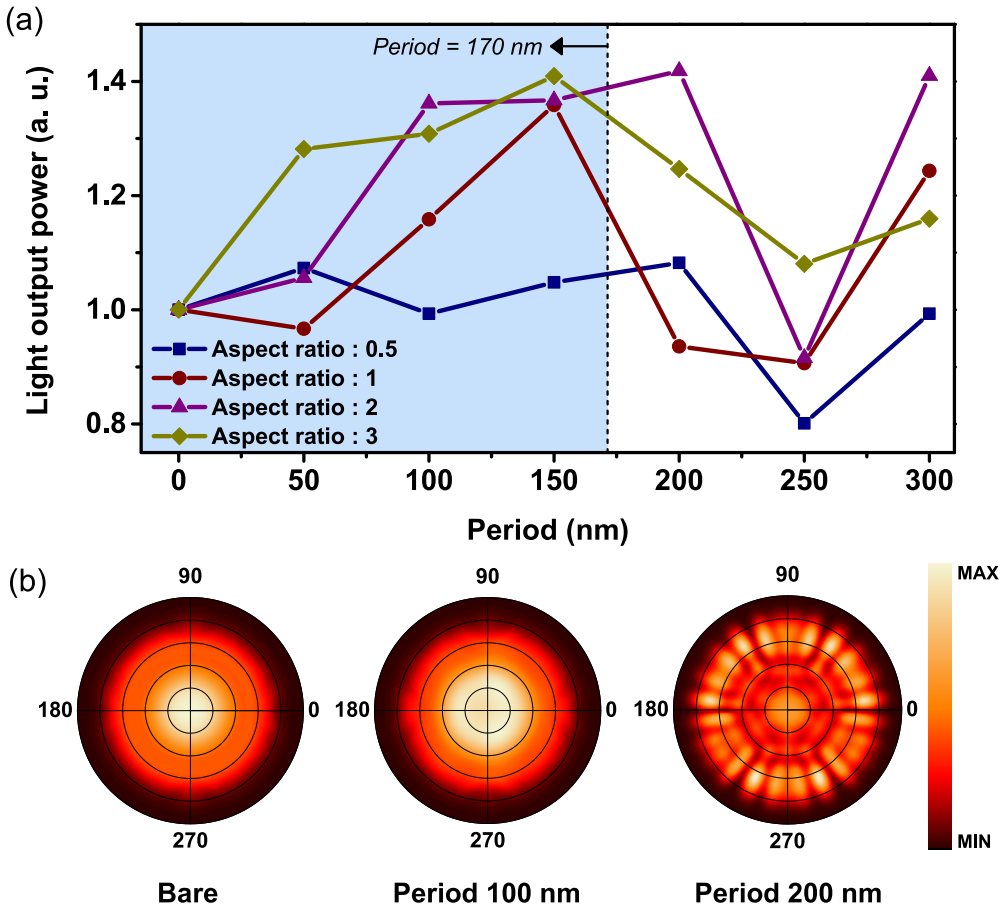

FIG. 4. (a) Calculated light output power of SWS-integrated LEDs with different periods (i.e., bare to 300 nm with 50 nm steps) for four different aspect ratios (i.e., 0.5, 1.0, 2.0, and 3.0). Blue-shaded areas indicate the subwavelength regions. (b) Simulated far-field patterns with an aspect ratio of 1.0 for bare (left), a period of 100 nm (center) and 200 nm (right), respectively.

the period of GaP SWSs for red LEDs should be below ~170 nm to achieve a high EQE without the higher order diffraction at any incident angle.

III. OPTIMUM DESIGN AND FABRICATION

To validate the results from the 3D RCWA and 2D grating equation, we simulated the light output power as a function of the period based on the three-dimensional FDTD method. Figure 4(a) shows the calculated light output power of the SWS-integrated LEDs with different periods and aspect ratios (ARs). In the subwavelength regime (i.e., the blue-shaded area), the light output power increases as the period increases. These improvements cannot be found in the SWSs with an AR of 0.5 because of the abrupt change of the effective refractive index. Except for the AR of 0.5, the maximum output power at subwavelength ranges can be achieved in the SWS-integrated LEDs with a period of 150 nm, with an enhancement factor of ~1.4. In the period of 200 nm to 300 nm, destructive/constructive interference of the diffracted light occurs depending on the period. Figure 4(b) supports our expectation about the light distribution of LEDs with nano-patterns. The SWS-integrated LEDs with a period of 100 nm show a uniform light distribution with improved light intensity compared with that of the LEDs with flat surface. Figure in the right part of Fig. 4(b) shows that higher order diffraction transforms light distribution patterns from uniform to non-uniform. These analyses provide guidance for the design of SWSs fabricated on the LEDs.

In order to confirm the viability of our theoretical analysis, we fabricated disordered SWS-integrated red AlGaInP LEDs (λ = 633 nm) by lithography-free dry etching of Ag nanoparticles. Although the structures fabricated by this method have no periodicity, the average distance/diameter of structures can be easily controlled by adjusting the annealing temperature and thickness of the Ag film.[19–21] It is also noted that the calculation of periodic SWSs is enough to show the tendency and optimum design of the random SWSs.[22] For the fabrication process, the AlGaInP LED epitaxial layers were grown by metal-organic chemical vapor deposition (MOCVD) on GaAs in the conventional 'p-side up' mode. The epitaxial structure consisted of a Si-doped n-type GaAs, 16 pairs of AlAs/AlGaAs distributed Bragg reflectors (DBRs), 20 pairs of GaInP/AlGaInP MQWs surrounded by a Te-doped n-type and Mg-doped p-type AlGaInP cladding layer, and an 8 μm thick Mg-doped p-type GaP window layer. The MOCVD-grown wafer was metallized using Ni/Au/Ge/Ni/Au on the n-side and AuBe/Au on the p-side for the LEDs. The fabricated LEDs have a dimension of 1 ×1 mm^2 Then, to reduce the internal Fresnel reflection for improving the outcoupling, disordered SWSs-integrated GaP window layers were fabricated by inductively coupled plasma - reactive ion etching (ICP-RIE) with thermally dewetted Ag nanoparticles. From the scanning electron micrograph (SEM) images (Fig. 5(a)) and the post image processing (Fig. 5(b), ImageJ, NIH, USA), it is found that the average distance and average size of the fabricated SWSs are 121.10 nm and 121.72 nm, respectively, which are close to the optimal period in the calculation. The heights of the SWSs are estimated to be in the range of 100–200 nm, from the tilted view of SEM image.

Fig. 5(c) shows the light output power–current–voltage (L–I–V) characteristics of the fabricated LEDs. Light output power measurement was carried out at the chip scale with an integrating sphere. The AlGaInP LEDs were operated under the DC bias condition at room temperature. It is found that the light output power of LEDs with and without SWSs are 20.65 mW and 14.32 mW, respectively, at a bias current of 200 mA. The enhancement ratio of the light output power is 1.44, which is comparable to the calculation result (i.e., 1.37 at a period of 150 nm and AR of 1.0), shown in Fig. 4(a). The inconsistency between measurement and calculation may result from the absence of DBR in the calculation, the structural differences such as the periodicity of SWSs, and the dimension differences. Fig. 5(d) shows the electroluminescence (EL) spectra of the conventional LED and the LED with SWSs at a driving current of 200 mA. Peak wavelengths of the conventional

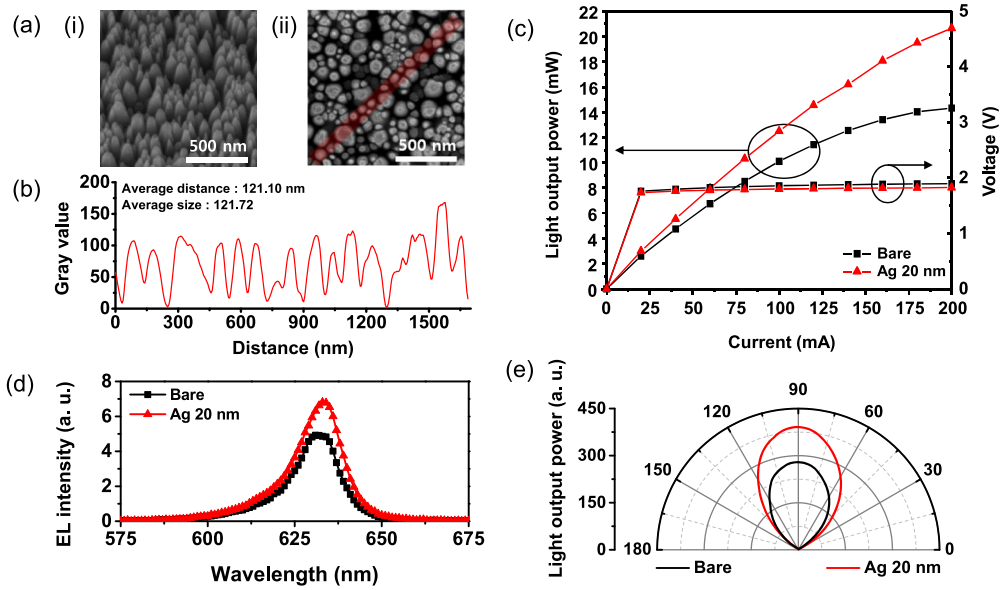

FIG. 5. (a) SEM images of the fabricated SWSs with the thickness of Ag 20 nm film: (i) tilt view, (ii) top view. (b) The gray value from the red line in the top SEM image providing adjacent distances and sizes of SWSs. (c) Light–current–voltage (L–I–V) characteristics of the SWS-integrated LEDs with different surface morphologies. The test was done after encapsulation. (d) Room temperature EL intensity of LEDs at 200 mA injection current. (e) Experimentally measured radiation patterns of LEDs.

and SWS-integrated LED are around 626 and 633 nm, respectively. The emission spectra of the SWS-integrated LED are very similar to the conventional LED except for the intensity level. Such behavior can also be found in the light output radiation patterns shown in Fig. 5(e). Because of the angle dependence of DBR, the radiation patterns of the LED with SWSs have a slight bias in the forward direction. The uniform radiation pattern with improved intensity in all direction indicates that the fabricated LEDs with SWSs are well designed and have an optimal structure.

IV. CONCLUSION

We performed a theoretical analysis of SWSs on GaP substrates by RCWA, FDTD, and 2D grating equation for achieving a high light output power with uniform light distribution. From these results, we found that the SWS period that ensures zeroth-order regime for all directions should be selected by considering several factors such as the substrate materials and emission wavelength. In case of GaP substrate at the wavelength of 633 nm, the SWS period of less than ~170 nm is needed to practically ensure the zero-order regime. Moreover, the period should be in the range of 100–150 nm to maximize the light output power of the LEDs, while maintaining the uniform light field distribution. To validate our theoretical analysis, we fabricated AlGaInP-based red LEDs with disordered SWSs by overall thermal dewetting process and dry etch process. The light output power enhancement of an LED with SWSs is ~1.44 times that of conventional LED, without any degradation of electrical properties. Moreover, the radiation pattern of the LED with SWSs shows a uniform light distribution with a slight bias in the forward direction because of the angle dependent property of DBR. This uniform radiation pattern of the LED with SWSs indicates that SWSs on GaP substrate by fabricated lithography-free process with Ag 20 nm are considered as the homogeneous medium, and the average period of disordered SWSs was distributed in the zeroth-order regime. We believe that these results provide guidance for the optimum design of surface-textured LEDs.

ACKNOWLEDGMENTS

This work was partly supported by the Basic Science Research Program of the National Research Foundation of Korea (NRF) funded by the Ministry of Science, ICT and Future Planning (2014R1A1A1005945), and by supported by MSIP as GFP / (CISS-2013M3A6A6073718).

[1] R.R. Willey, Appl. Opt. **50**, C274 (2011).
[2] A. Deinega, I. Valuev, B. Potapkin, and Y. Lozovik, J. Opt. Soc. Am. A. Opt. Image Sci. Vis. **28**, 770 (2011).
[3] B.U. Ye, B.J. Kim, Y.H. Song, J.H. Son, H.K. Yu, M.H. Kim, J.L. Lee, and J.M. Baik, Adv. Funct. Mater. **22**, 632 (2012).
[4] D. Poitras and J.A. Dobrowolski, Appl. Opt. **43**, 1286 (2004).
[5] Y.T. Lee, Y.M. Song, S.J. Jang, and J.S. Yu, Small **6**, 984 (2010).
[6] A. Gombert, W. Glaubitt, K. Rose, J. Dreibholz, B. Bläsi, A. Heinzel, D. Sporn, W. Döll, and V. Wittwer, Thin Solid Films **351**, 73 (1999).
[7] K. Kintaka, J. Nishii, A. Mizutani, H. Kikuta, and H. Nakano, Opt. Lett. **26**, 1642 (2001).
[8] W.-L. Min, B. Jiang, and P. Jiang, Adv. Mater. **20**, 3914 (2008).
[9] Y.H. Kang, S.S. Oh, Y.-S. Kim, and C.-G. Choi, Microelectron. Eng. **87**, 125 (2010).
[10] S. Chattopadhyay, Y.F. Huang, Y.J. Jen, a. Ganguly, K.H. Chen, and L.C. Chen, Mater. Sci. Eng. R Reports **69**, 1 (2010).
[11] R. Brunner, O. Sandfuchs, C. Pacholski, C. Morhard, and J. Spatz, Laser Photonics Rev. **6**, 641 (2012).
[12] Y.-F. Huang, S. Chattopadhyay, Y.-J. Jen, C.-Y. Peng, T.-A. Liu, Y.-K. Hsu, C.-L. Pan, H.-C. Lo, C.-H. Hsu, Y.-H. Chang, C.-S. Lee, K.-H. Chen, and L.-C. Chen, Nat. Nanotechnol. **2**, 770 (2007).
[13] Y.M. Song, E.S. Choi, J.S. Yu, and Y.T. Lee, Opt. Express **17**, 20991 (2009).
[14] Y.M. Song, G.C. Park, S.J. Jang, J.H. Ha, J.S. Yu, and Y.T. Lee, Opt. Express **19 Suppl 2**, A157 (2011).
[15] E.K. Kang, E. Kwon, J.W. Min, Y.M. Song, and Y.T. Lee, **02**, 4 (2015).
[16] Y.M. Song, Y. Jeong, C. Il Yeo, and Y.T. Lee, Opt. Express **20**, A916 (2012).
[17] W.S. Cheung, Y.F. Cheung, H.T. Chen, R.S.Y. Hui, and E. Waffenschmidt, Opt. Express **23**, 15021 (2015).
[18] F. Falco, T. Tamir, and K.M. Leung, J. Opt. Soc. Am. A **21**, 1621 (2004).
[19] Y.M. Song, E.S. Choi, G.C. Park, C.Y. Park, S.J. Jang, and Y.T. Lee, Appl. Phys. Lett. **97**, 9 (2010).
[20] Y.T. Lee, Y.M. Song, J.H. Jang, J.C. Lee, and E.K. Kang, Sol. Energy Mater. Sol. Cells **101**, 73 (2012).
[21] E.S. Choi, Y.M. Song, G.C. Park, and Y.T. Lee, J. Nanosci. Nanotechnol. **11**, 1342 (2011).
[22] C. Lin, N. Huang, and M.L. Povinelli, Opt. Express **20**, 125 (2012).